DESIGN AND TESTING OF A LOW SUBSONIC WIND TUNNEL GUST GENERATOR

P.M.G.J. Lancelot[1], J. Sodja[1], N.P.M. Werter[1], and R. De Breuker[1]

[1] Delft University of Technology
Kluyverweg 1, 2629 HS Delft, The Netherlands
R.DeBreuker@tudelft.nl

Keywords: Gust generator, computational fluid dynamics, fluid structure interaction, experimental aerodynamics, experimental aeroelasticity

Abstract: This paper summarises the design of a gust generator and the comparison between high fidelity numerical results and experimental results. The gust generator has been designed for a low subsonic wind tunnel in order to perform gust response experiments on wings and assess load alleviation. Special attention has been given to the different design parameters that influence the shape of the gust velocity profile by means of CFD simulations. Design parameters include frequency of actuation, flow speed, maximum deflection, chord length and gust vane spacing. The numerical results are compared to experimental results obtained using a hot-wire anemometer and using flow visualisation by means of smoke. Discrepancies have been noticed between CFD and flow measurements but trends compare well and the system is fully functional.

1 INTRODUCTION

Gust encounter is among the most critical load cases an aircraft can encounter. The increasing aspect ratio of modern commercial aircraft wings and weight reduction generally result into an increased wing sensitivity to gust loads. Researchers have been looking for solutions to reduce structural stresses at the wing root caused by gust encounters, either by using passive (e.g. aeroelastic fibre and thickness tailoring) or active methods (e.g. active control surfaces). Reducing loads can effectively reduce the weight and hence operational cost of the aircraft. In order to ease the development of these methods, many computational techniques of different fidelity levels have been developed to evaluate the structural response to gust loads. Nonetheless, the unsteady nature of gust flow and strong coupling with structural deformations make the dynamic response modelling a challenging task. Hence code validation is necessary. The construction of a gust generator is required for gust loads experiments in a wind tunnel and many research institutes and universities have been building similar systems for the purpose of their own research. Different ways of producing gust have been explored, such as rotating slotted cylinder [1] or by the pitch oscillation of one or multiple airfoils [2-7]. The first method has the advantage that it requires very low torque and power input while the second one needs to oscillate entire gust vanes. On the other hand, the flow produced by the second method is easier to evaluate numerically. The development of a device of this kind is driven by the performance required by the experiment itself and by the wind tunnel facilities available. The wind tunnel used at the Delft University of Technology is the Open Jet Facility, which features a test section of 2.85x2.85 m and can reach a flow speed of 35m/s. Our goal is to produce a discrete gust to evaluate load alleviation and gust response

of tailored composite wings, as shown in Figure **1**. This paper presents the development of the gust generator as well as the generation of a sine wave gust.

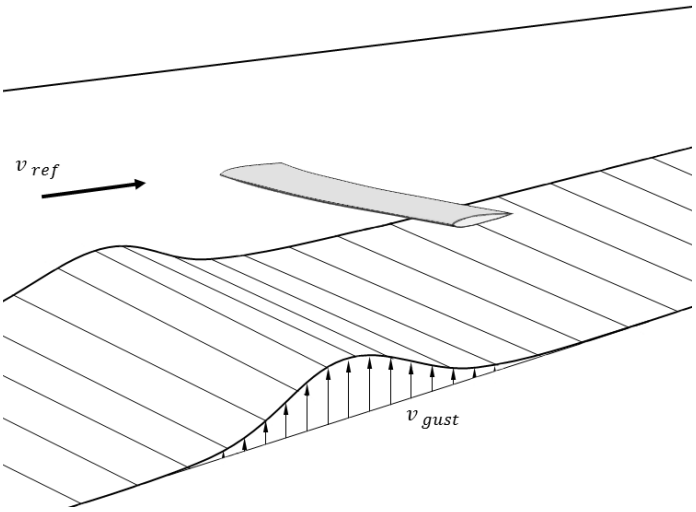

Figure 1: The generator intends to reproduce discrete gust in the wind tunnel for load alleviation experiment on a semi-wing with a free end tip. v_{ref} is the free stream flow speed and v_{gust} the gust speed.

2 PRELIMINARY DESIGN STUDY

This section starts by presenting the requirements and the preliminary use of CFD simulations in order to identify the key design parameters and optimise gust generator performance. Design parameters include the frequency of actuation, the flow speed, the maximum deflection, the chord length of the gust vanes and the spacing between these two. After this, the wind tunnel and the overall setup are presented. Fluid-structure interactions (FSI) simulations are done to evaluate the structural behavior of the gust generator. Finally the actuation system will be presented as well.

2.1 Requirements

The gust generator target performance is based on the CS23 certification from the European Aviation Safety Agency (EASA) [8]. Accordingly, the evolution of the amplitude of a discrete gust is defined as follows:

$$v_{gust} = \frac{v_G}{2}\left(1 - \cos\frac{2\pi s}{25\bar{C}}\right) \tag{1}$$

where v_G denotes the maximum gust amplitude, *s* the distance traveled by the aircraft inside the gust, and $\bar{C}$ its mean chord. It is possible to deduce the gust frequency *f* that needs to be attained inside the wind tunnel from *s*

$$s = v_{ref} \cdot t \tag{2}$$

$$\frac{v_{ref}}{25\bar{C}} = f \tag{3}$$

The maximum speed allowed in the wind tunnel for this type of experiment is 25 m/s, therefore v_{ref} is here equal to 25 m/s. Beside the flow speed, the frequency is also function of the mean chord $\bar{C}$ of the aircraft that encounters the gust. The future test wing will have a chord length varying from 0.2 m to 0.4 m. For this range, the needed gust frequencies are:

$$f = \frac{25}{25 \cdot [0.2,0.4]} = [5,2.5] \tag{4}$$

To comply with the gust requirement from the EASA certification, it is then necessary to reach a gust frequency of 5 Hz at a flow speed of 25 m/s. Most of the results in this paper are formulated with respect to the gust angle, which allows a comparison of the change in angle of attack induced by the gust at different flow speeds:

$$\alpha_{gust} = \tan^{-1}\left(\frac{v_{gust}}{v_{ref}}\right) \tag{5}$$

2.2 Preliminary Study of the Gust Generator

The gusts are produced by two rectangular gust vanes (with a symmetric airfoil) oscillating in pitch around their ¼ chord axis. Comparisons between flow measurements and simulations from [2,3,5] have shown that having two gust vanes is a good compromise between gust quality and setup complexity. The gust uniformity is critical to ensure the repeatability of the experiment and makes the gust response of the wing easier to compute. In the *DLR* experiment [3], having only one gust vane penalises the uniformity of the gust in space, since an important shear flow region due to the airfoil boundary layer is created in the wake behind the gust generator. Adding a second gust vane, with the test wing in-between avoids this effect. The shear flow region can be observed Figure 2. Going for more than 2 gust vanes is a good solution to further increase the gust uniformity, but the shear flow area in the wake can be a problem again if the model to test doesn't fit in-between.

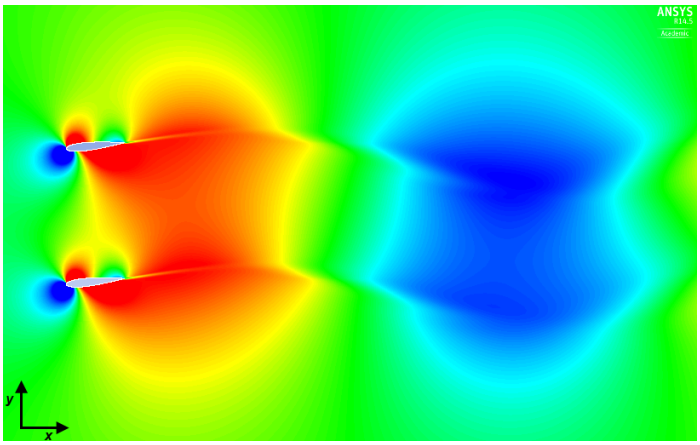

Figure 2: Contours of the gust angle for a time transient CFD simulation with ANSYS Fluent.

2D time transient flow simulations are done to evaluate how the gust flow reacts to different types of gust vane motion and geometry. ANSYS Fluent is used, with a pressure based solver and the Spalart-Allmaras turbulence model. The time step size is set to 0.002 seconds after a convergence study on the size of this parameter. For the sake of simplicity, the full interior of the Open Jet Facility is not modeled. The mesh shown in Figure 3 and 7 uses 100.000

deformable rectangular elements and is obtained after a convergence study. The motion of the vanes is directly simulated by moving the boundaries of the airfoils, around a point located at the quarter chord using FLUENT's user defined functions (UDFs).

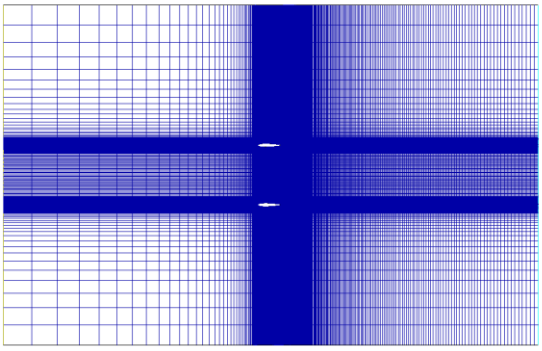

Figure 3: Structured 2d grid.

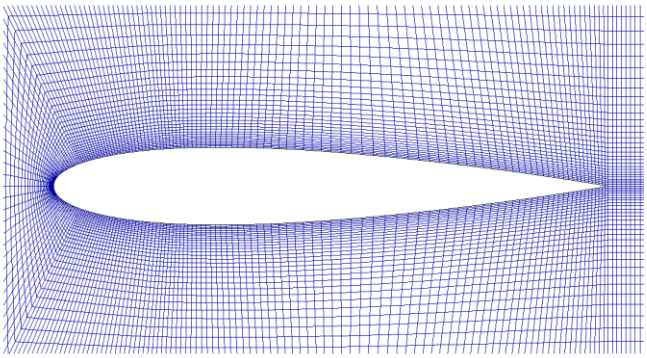

Figure 4: Close up on one of the two gust vanes.

Many design variables are available when it comes to building a gust generator; they are summarised in Table 1:

Design variables	Values evaluated
Chord length of the gust vanes: c	0.2 m, 0.3 m, 0.4 m
Space between the gust vanes: dh	0.3 m, 0.5 m, 0.7 m
Reduced frequency: $k(f,v_{ref})$	0.0377, 0.113, 0.1884
Maximum angle of deflection of the gust vanes: δ_{max}	2.5, 5, 10 degrees

Table 1: Design variables.

The vane chord length c can't be changed during the experiment. The spacing dh between the two vanes can normally be adjusted, but due to time constraints, only one configuration is studied in the experiment. The influence of these parameters is evaluated purely numerically. In Figure 5, simulations are being run at constant flow velocity and frequency of actuation, and the only variable is the chord length of the gust vanes. It is clear that a linear relation exists between the maximum gust angle, α_G, and the chord length.

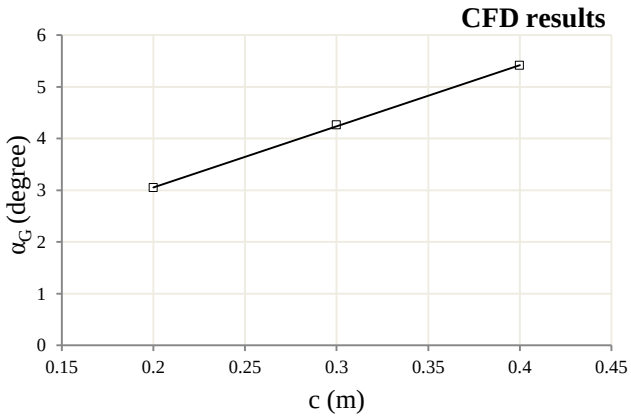

Figure 5: The maximum gust angle measured for different chord lengths. These measurements are taken 1.5 m behind the leading edge of the gust vanes, in the center axis of the fluid domain. $\delta_{max} = \pm 10$ degrees.

The next parameter under investigation is the spacing between the gust vanes. The flow interaction between two gust vanes has already been studied numerically by *Dequand et al.* [2] and they concluded that some interaction can occur, if the two vanes are too close, which alters the shape of the gust. Similar observations can be made in Figure 6, showing a change in the shape of the gust profile as the vanes get closer. Figure 7 shows the gust velocity profile in the transverse direction at two different times for dh = 0.7 m and dh = 0.3 m. It can be observed that the area in-between "swings" around the 0 position. This effect is more pronounced at dh = 0.3m, and a model located behind the gust generator will always be subjected to the shear flow region. Hence, having a larger spacing between the two gust vanes is more suitable for the quality of the experiment. Flow interactions are also noticeable on Figure 2.

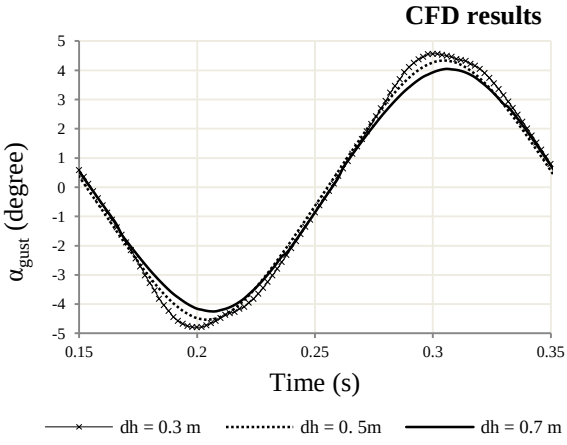

Figure 6: Gust angle in time, for different vane spacing. c = 0.3 m, v_{ref} = 25 m/s, f = 5 Hz and δ_{max} = ±10 degrees.

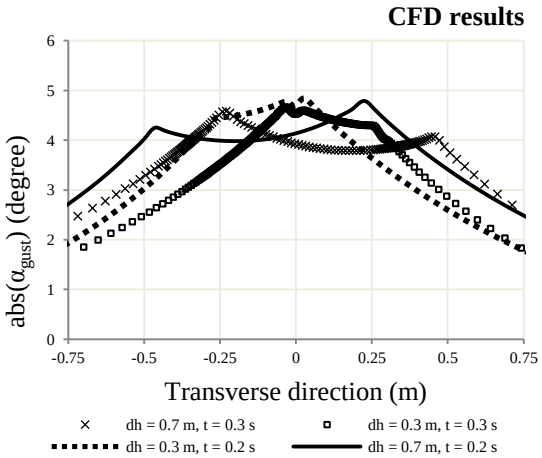

Figure 7: Gust amplitude variation in the transverse direction for different vane spacing. Same conditions as Figure 6.

Next, the gust angle is also dependent on the reduced frequency *k* which is defined as:

$$k = \frac{\omega c}{2v_{ref}} \tag{6}$$

Where ω is the frequency in *rad/s*, and the *c* chord length of the vanes. c is constant and equal to 0.3 m for the following results. A test matrix has been defined to evaluate both numerically and experimentally the effect of reduced frequency at different flow speeds, as given in Table 2:

Reduced frequency *k*	Wind tunnel reference speed v_{ref}		
	15 m/s	21 m/s	25 m/s
0.0377	*f = 0.6* Hz	*f = 0.84* Hz	*f = 1* Hz
0.1130	*f = 1.8* Hz	*f = 2.52* Hz	*f = 3* Hz
0.1884	*f = 3* Hz	*f = 4.2* Hz	*f = 5* Hz

Table 2: Operational actuation frequency and flow speed

In Figure 8, it can be clearly seen that the same reduced frequency at different flow speeds, results in the same gust amplitude. Furthermore, it can be seen that the gust angle varies depending on the distance behind the gust generator. Finally the influence of the maximum

deflection is investigated. There is a linear relation between deflection angle and the maximum gust angle observable in Figure 9. As expected, results with k = 0.1884 are higher.

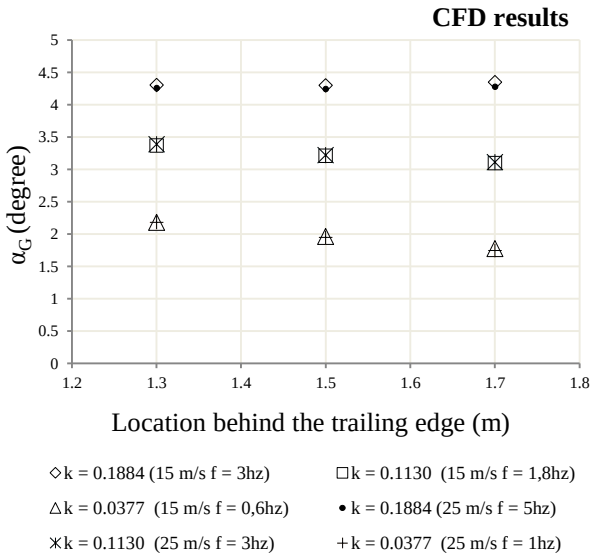

Figure 8: The maximum gust angle measured at 3 different locations and reduced frequency. δ_{max} = ±10 degrees.

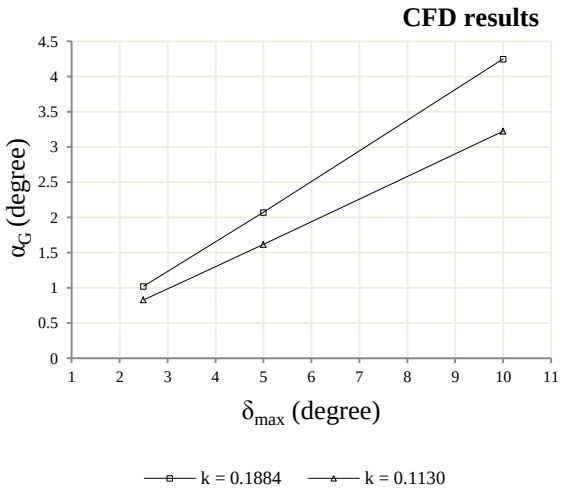

Figure 9: The maximum gust angle measured with 3 different δ_{max} and 2 reduced frequencies.

The preliminary CFD study supports the evidence that gust amplitude is linked linearly with the vane chord length and the maximum deflection angle. Increasing the reduced frequency induces stronger a gust as well. Similarly, this is observed with a smaller spacing between the two gust vanes but leads to discrepancies in the gust flow, which can alter the quality of the experiment.

2.3 Open Jet Facility

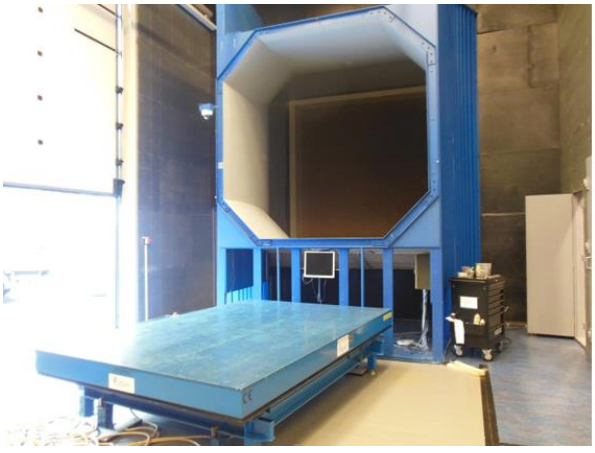

Figure 10: Interior of the Open Jet Facility at TU Delft.

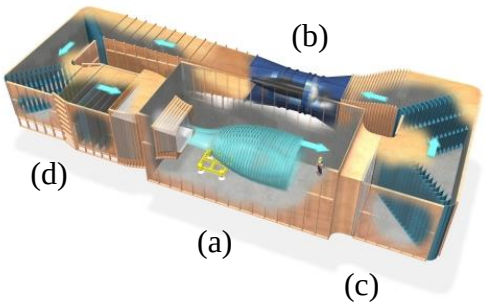

Figure 11: Schematic of the OJF's closed circuit. (a) is the test chamber, (b) the turbine, (c) the cooling system and (d) the grids and filters to reduce turbulence in the flow.

The Open Jet Facility (OJF) at Delft University of Technology is a low subsonic wind tunnel powered by a 500 kW turbine. The test section as shown in Figure 10 has a width and height of 2.85 m. The measurement equipment can be directly installed next to the experiment,

which makes this wind tunnel versatile and convenient to use. The closed circuit of the OJF, shown in Figure 11, allows the wind speed to go up to 35 m/s continuously in a controlled temperature environment.

2.4 Design of the Frame

As shown in Figure 12, the frame is made of aluminium rectangular and extruded profiles. The truss members are joined using bolts, T-slot nuts, bracket and specially designed attachment plates. The frame supports the gust vane and the actuators. It is designed to not interfere with the flow, and therefore bypasses the flow inlet of the wind tunnel. The gust vanes are currently mounted vertically onto the frame, but they can also be mounted horizontally.

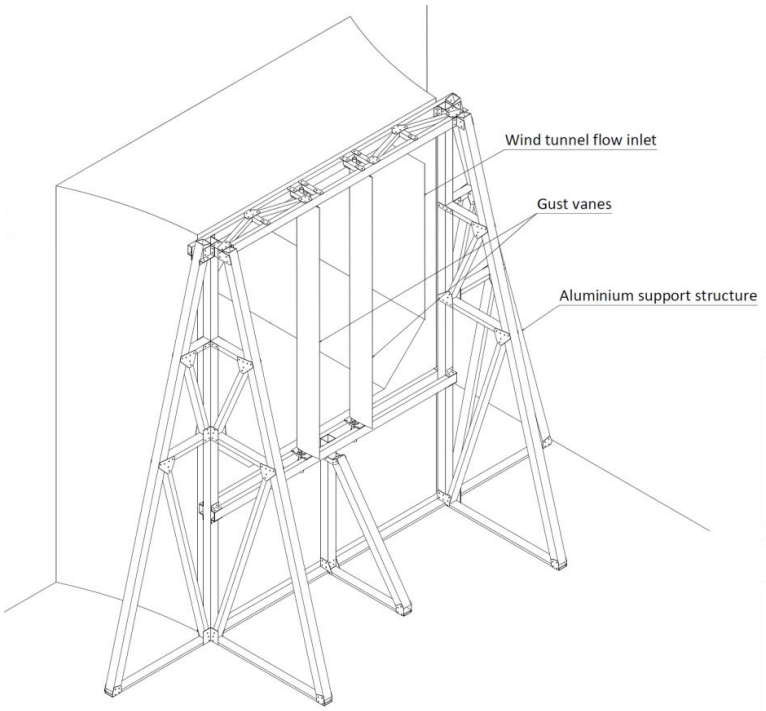

Figure 12: Sketch of the design of the gust generator and how it is positioned in the Open Jet Facility.

One of the design challenges is to ensure that the frame will not resonate with the operational frequency bandwidth of the gust vanes. For that purpose, numerous finite element simulations using a simplified beam element model have been done to obtain the present design. The frame is designed to be bolted on the ground. With this configuration, the first natural frequency shown in Figure 13, is 28.4 Hz and is high enough to not resonate with the gust vane motion. However for this first experimental session with the gust generator, the frame isn't attached to the ground. The natural frequencies of this new configuration are evaluated with a model featuring only two attachment points, the weight of the frame (200 kg) still providing grip with the ground. As can be observed in Figure 14 and Figure 15, the resulting Eigen frequencies are significantly lower. The first and second modes are at 3.4 Hz and 4.5 Hz. The first mode isn't an issue either considering its shape and the direction in which the aerodynamic forces are acting (the lift from the gust vanes is along the *y* axis). Thus, it has been decided to limit the operational frequency of the gust generator to 4.2 Hz, since the frame is not fully attached on the ground.

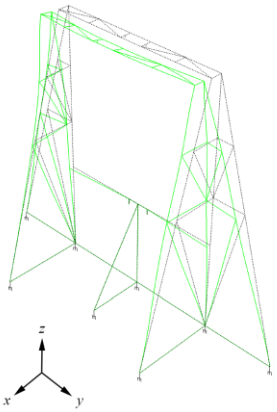

Figure 13: First mode at 28.4 Hz. The frame is fully attached on the ground.

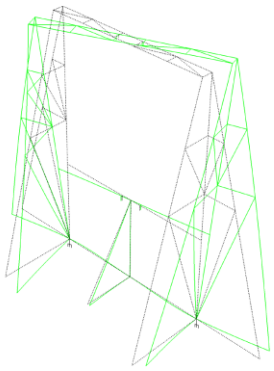

Figure 14 : First mode shape at 3.4 Hz with only two attachment points on the ground.

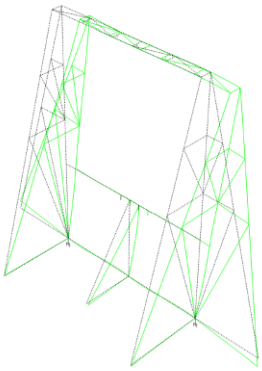

Figure 15: Second mode shape at 4.5 Hz with only two attachment points on the ground.

2.5 Design of the Vanes

The gust vanes are made from Evonik ROHACELL 31IGF foam. This foam allows for a lightweight design and offers good machinability. The surface is impregnated with epoxy resin to increase its toughness and regularity. During operation, the gust vanes are under high inertia and aerodynamic forces (up to 300N of static load) and it is necessary to ensure that they will not bend or twist, because this could also affect the flow quality. The airfoil thickness (0.042 m with a NACA0014 airfoil) is chosen in order to fit an aluminium spar inside, to provide the necessary stiffness, as illustrated in Figure 16 and Figure 17. The vanes are 2.88 m long, to cover the full height of the wind tunnel, and to avoid having any support structure in the flow. The chord length is 0.3 m to provide enough gust amplitude.

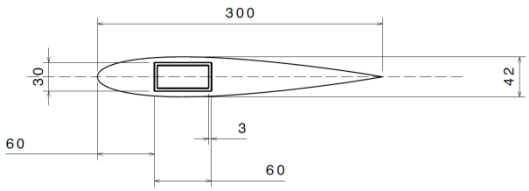

Figure 16: Dimension of the vane section in mm. The airfoil is a NACA0014.

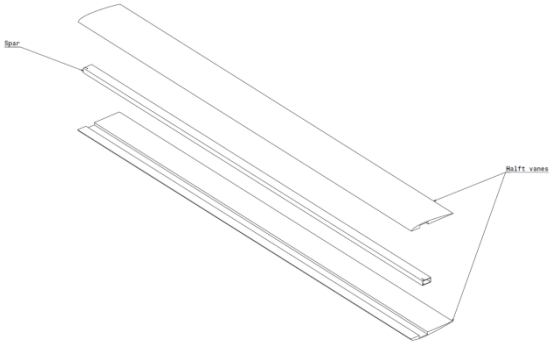

Figure 17: Two “half vanes” and the aluminium spar.

In order to ensure that the vanes will not experience any resonance vibrations due to their own motion, modal analyses are performed. The vane is clamped at one end (simulating the actuator), and free to rotate at the other end. The first mode, in bending, is at 21 Hz and deemed far enough from the actual frequency of actuation to avoid resonance. Additional high fidelity coupled fluid/structure simulations using ANSYS CFX/Structural are done to evaluate the deformation of the gust vanes under unsteady aerodynamics loads and inertia loads as represented in Figure 18, and evaluate the required torque from the actuators. These simulations are done in 3D, with a structured mesh of 6 million hexahedral elements using similar parameters as the simulations previously done in 2D for the CFD part. Walls are

located at each ends of the gust vanes to prevent any wingtip vortices. For each vane, the structural model is composed of 6000 non-linear wedge elements for the foam core, and 600 shell elements for the aluminium spar. The simulations are run at a higher flow speed (35 m/s) and frequency of oscillation (10 Hz) than for the experiment, in order to assess the vanes design robustness. Their deformations in bending and torsion are monitored at different span wise locations.

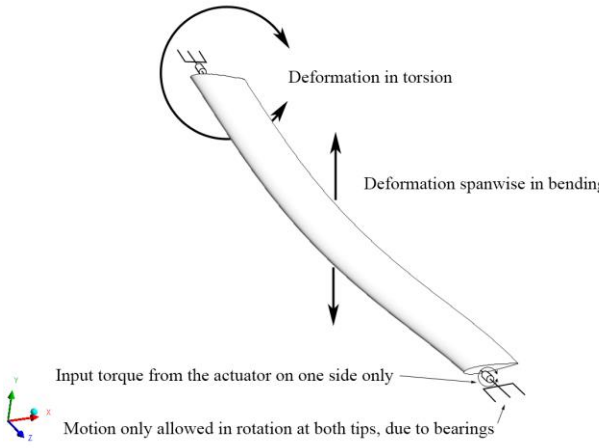

Figure 18: Schematic of the deformation that a gust vane can experience under inertia and aerodynamic forces.

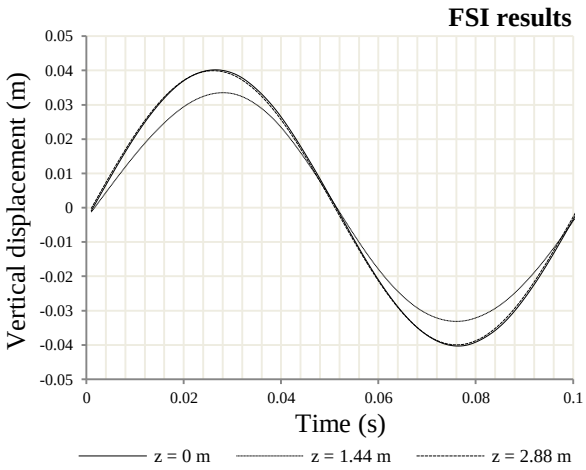

Figure 19: Measurements in time at 3 points located on the trailing edge at both vanes tip and at mid span.

The vertical displacement of the trailing edge is measured to monitor deformations of the gust vane. The trailing edge is located at a distance of 0.229 m from the axis of rotation of the vane and normally experiences a vertical displacement with an amplitude of ± 0.04 m when the vane is oscillating without any structural deformation and with δ_{max} = ±10 degrees. As can be seen in Figure 19, the measurement point located at mid span (z = 1.44 m), varies with less amplitude (about 7mm) than the two others measurement points at the tips. This is due to the bending in span wise direction from the lift, while torsion (mainly due to inertia loads) is however less noticeable, because most loads are taken by the aluminium spar. To measure the impact of the vane deformations on the flow, the gust speed is measured at five locations 1.5 m behind the gust generator, in between the two vanes. Figure 20, shows a side-view of the wake trailing the gust vanes at the center in between vanes showing small span wise gust flow discrepancies. Figure 21 shows the gust velocity profiles taken at five different span wise locations behind the gust generator, and they are all very similar. Thanks to the FSI simulations, it is proved that the design of the vanes is strong enough to not break, and to not excessively disturb the flow when deforming under the loads.

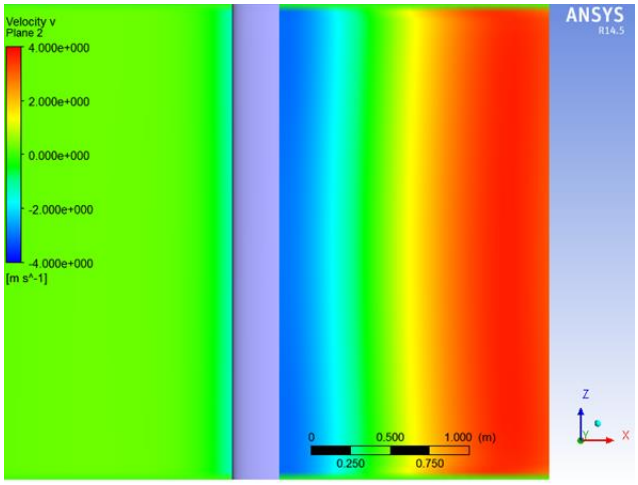

Figure 20: Contours of the gust angle for a time transient FSI simulation.

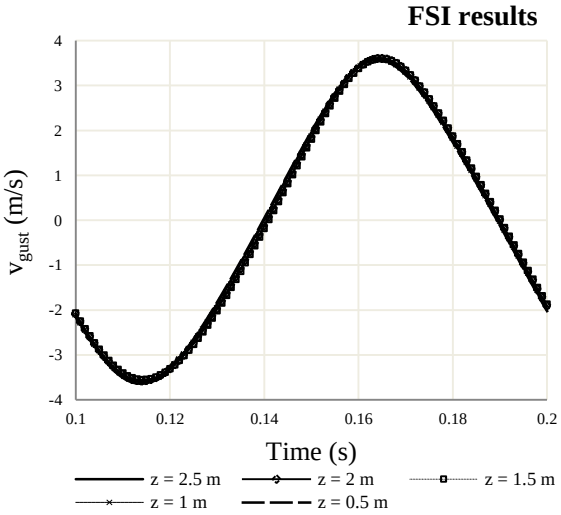

Figure 21: Velocity profile taken at five different span wise locations behind the gust generator.

2.6 Actuators and Control

The actuators selected to rotate the vanes are built by Applied Motion and their specifications are given in Table 3. A gearhead with a 25:1 gear ratio was selected to increase the delivered torque.

Motors	
Operating voltage	48V
Nominal current	5.8 Amps
Peak current	14 Amps
Nominal torque	0.56 N.m
Rated speed	3350 RPM
Gearheads	
Gear ratio	25:1
Maximum input speed	5000 RPM
Maximum output torque	30.71 N.m
Servo drives	
Operating voltage	48V
Nominal current	7 Amps
Peak current	14 Amps
Power supply	
Power	320 Watts
Maximum output current	6.7 Amps

Table 3: Actuator specifications

Closed-loop control is implemented in LabVIEW to drive the actuators. Position feedback is achieved by using high-frequency laser distance sensors. This setup allows for fast and independent control of each vane.

3 EXPERIMENT AND RESULTS

In order to assess the performance of the gust generator, measurements are done for a range of flow speeds, frequencies of actuation, vane deflection amplitudes (± 2.5, ± 5 and ± 10 degrees) and locations (see Table 4 and Figure 22). Due to issues with the frame's attachment to the ground discussed in section 2.4, a revised test matrix without the 5 Hz measurements is used for the experiment:

Reduced frequency k	Wind tunnel reference speed v_{ref}		
	15 m/s	21 m/s	25 m/s
0.0377	$f = 0.6$ Hz	$f = 0.84$ Hz	$f = 1$ Hz
0.1130	$f = 1.8$ Hz	$f = 2.52$ Hz	$f = 3$ Hz
0.1884	$f = 3$ Hz	$f = 4.2$ Hz	

Table 4: Revised experimental test matrix

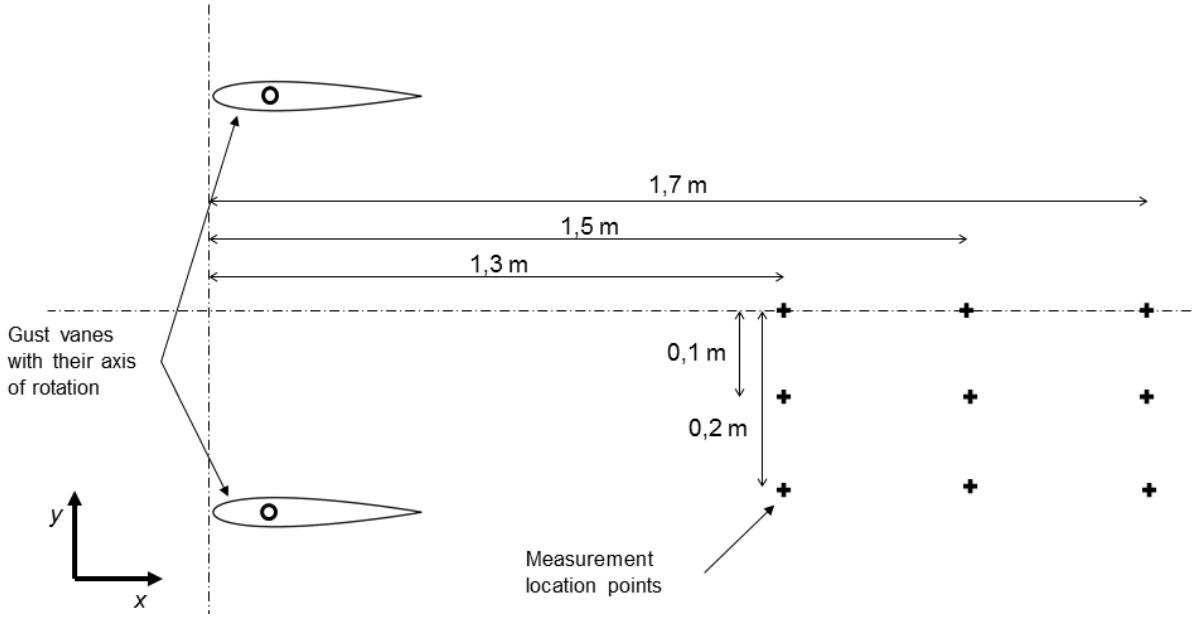

Figure 22: Schematic of the different positions for the measurements.

The first section will describe the experimental setup, followed by the way data are processed. Finally a comparison between the experimental results and the predictions from the CFD and visual observations are presented.

3.1 Experimental Setup

The system to measure the gust velocity uses a single hot wire anemometer, coupled with a pitot tube as shown in Figure 23 and Figure 24. This equipment is mounted on a traversing system, allowing measurements at different locations in space. Measurements are conducted at two different levels. The wingtip effect of the gust vanes is the lowest at z = 1.5 m, thus it is the most suitable height for a comparison with the 2D CFD. Measurements are also conducted at the height of z = 0.5 m to evaluate how the gust flow varies span wise.

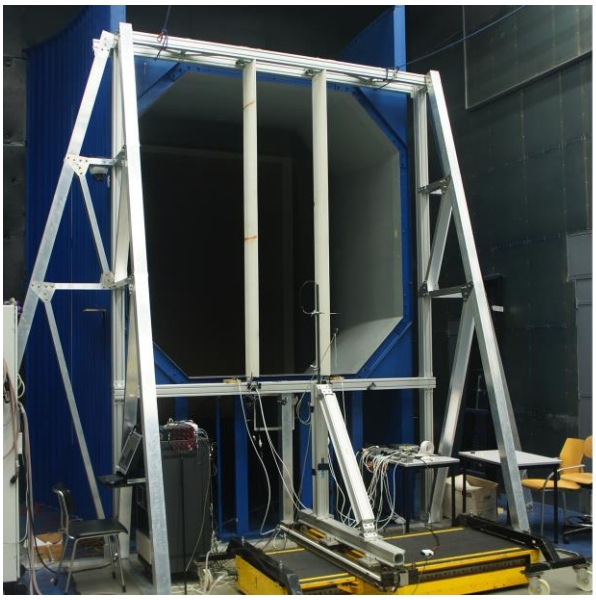

Figure 23: In yellow, the translation system.

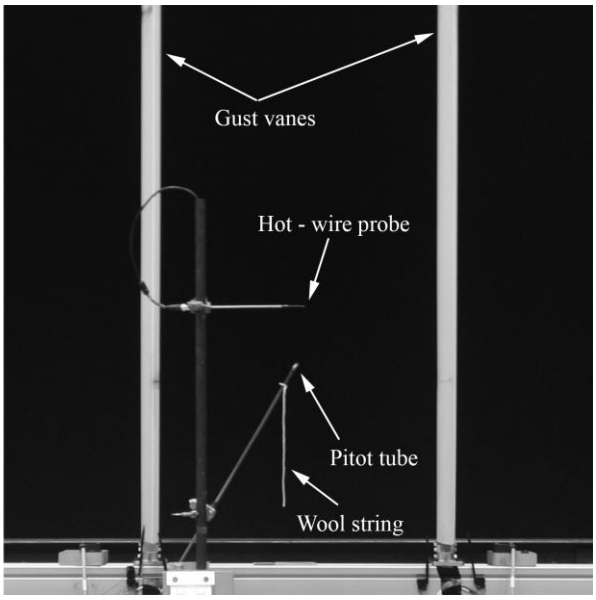

Figure 24: The hot wire anemometer in position at height z = 0.5 m.

The pitot tube is used to calibrate the hot-wire by providing the free-stream flow speed. The hot-wire measures the flow variations in the transverse direction induced by the gust generator. This type of anemometer measures the resistance of a thin-wire that has been heated to a certain temperature. As the flow flows past, the wire is cooled providing a measure for flow speed in the plane normal to the wire direction as indicated in Figure 25. Since the gust flow speed is much smaller than the principal flow speed, a cross-wire arrangement would be preferred to provide accurate measurements in two components. However, because of the availability of measurement equipment, only a single hot-wire was available, and, therefore the single hot-wire can be used as a qualitative measurement to evaluate trends, the exact gust amplitudes are most likely affected too much by the principal flow component.

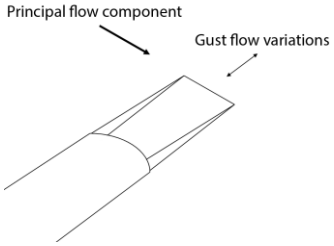

Figure 25: Schematic of the hot wire probe. The hot wire is used to measure flow variation normal to the wire direction.

3.2 Data Processing

The measurements with the hot wire are recorded over 30 seconds, at a sampling frequency of 10 kHz. As shown in Figure 26, the initial measurements have a low signal to noise ratio and a low pass filter is used to filter out a periodic signal and to read its amplitude and frequency. The low pass cut-off frequency is four time the actual frequency of actuation. It can be noticed that there are in fact two signals in the filtered data. First, the probe cannot make the distinction between positive and negative amplitude, so this doubles the frequency of the input signal, as shown in the FFT in Figure 27. Second, due to the probe's orientation (horizontal and perpendicular to the free stream flow), the gust flow measured is getting lowered in one direction and not in the other.

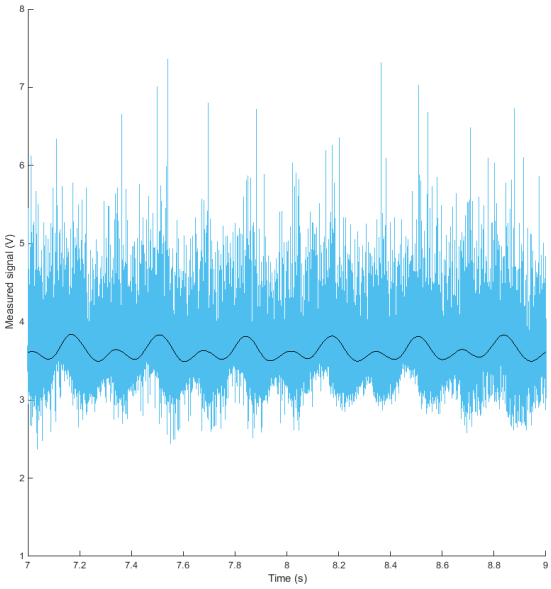

Figure 26: Raw data and the filtered signal in time.

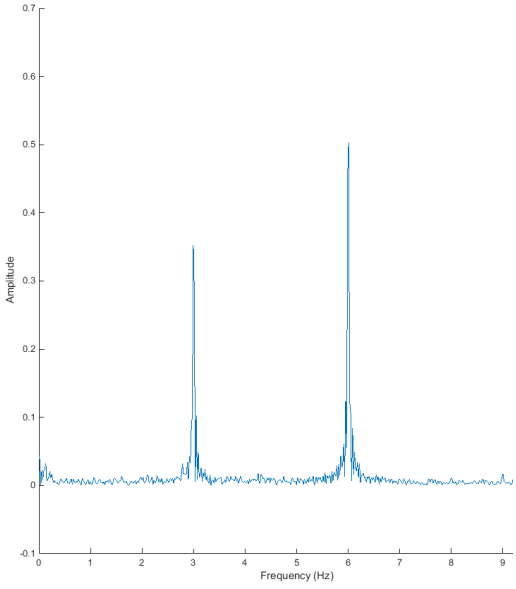

Figure 27: FFT on the raw signal after removing the baseline amplitude. In this example the actuation frequency is 3 Hz.

3.3 Comparison Between CFD and Experimental Results

In this section, the measured gust angle is compared to CFD predictions. CFD simulations predict that the gust amplitude scales linearly with the vane's maximum deflection and Figure 28 shows the same for the measurements. It can also be seen that a higher reduced frequency shows a slight increase in gust amplitude. Figure 29 shows comparison between numerical and experimental results for a gust amplitude (normalised with respect to the value of each series at $\delta_{max} = \pm 10$ degrees) and provide a qualitative comparison of the measured trends versus the expected trends, showing good agreement, thus providing some validation of the numerical results.

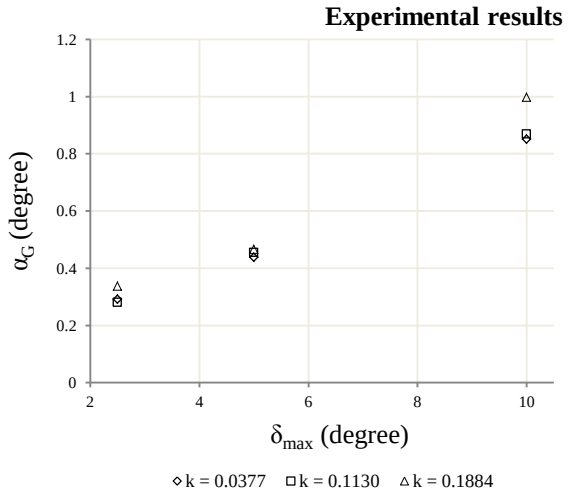

Figure 28: Maximum gust angle for different vane's deflection and reduced frequency. z = 1.5 m

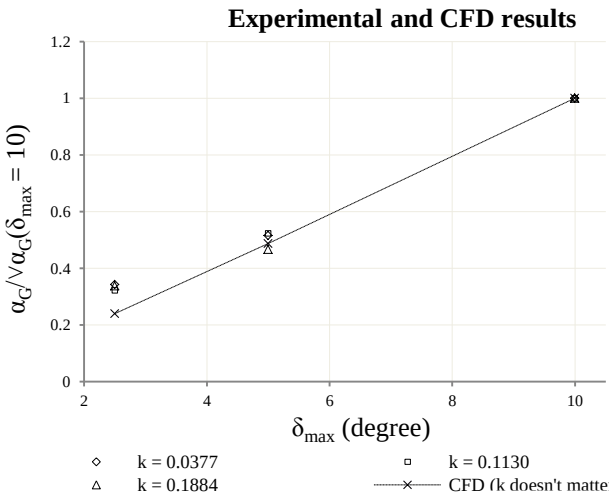

Figure 29: Normalised maximum gust angle for different vane deflection and reduced frequency.

As shown in Figure 30, the maximum gust angle varies behind the gust generator. Larger gust variations occur at z = 0.5 m. This is probably caused by the open jet inlet and can possibly be improved by using a lower wall at the inlet, preventing the air from falling when it leaves the inlet. As can be expected, at z = 1.5 m, the results in Figure 31 are more consistent with the 2D CFD results, and the gust angle variations are lower. Again, some variation occurs with reduced frequency but the effect of it is lower than predicted by the CFD simulations (see Figure 8) and gust the angle does not increase with the reduced frequency as much as seen with the simulations.

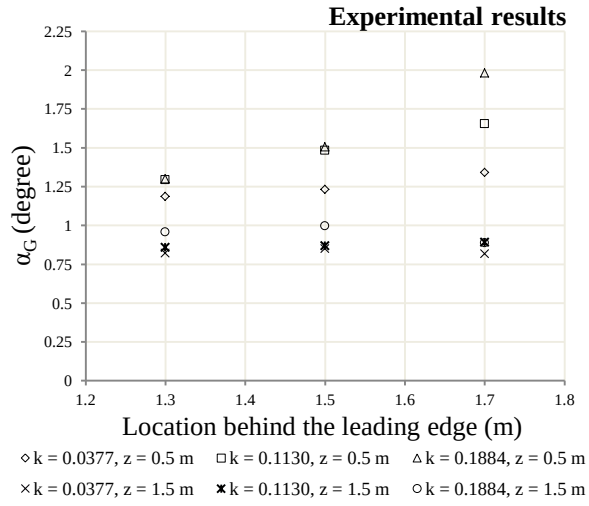

Figure 30: Maximum gust angle for different locations behind the gust vanes, heights and reduced frequency. δ_{max} = ±10 degrees.

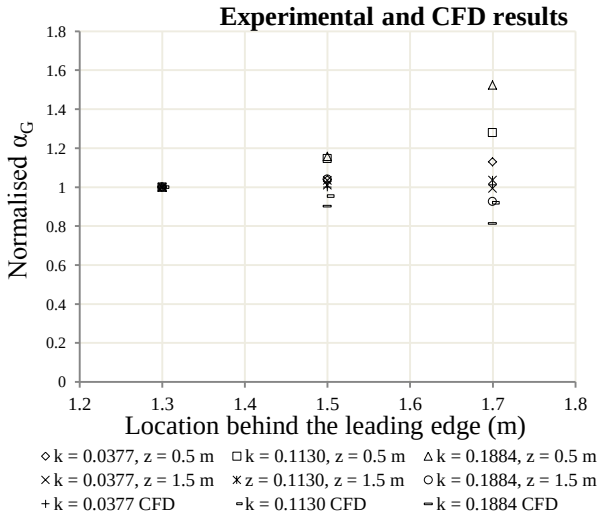

Figure 31: Same as Figure 30, but compared with the CFD results. The data are normalised with respect to the values at 1.3 m behind the leading edge for each series.

The gust angle at different locations in both transverse and longitudinal direction has also been evaluated, at 10 cm and 20 cm off-centre (see Figure 22). From Figure 32 to Figure 34, gust angles are plotted for different reduced frequency (k = 0.1884, k = 0.1130, k = 0.0377, from the top to the bottom surface), the position behind the gust generator (x direction) and the transverse position (y direction) for a maximum deflection angle of the vanes (δ_{max}) of ±10 degrees. The results are normalised for each plot with respect to their average gust angle.

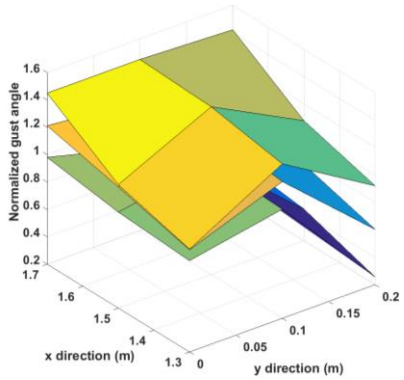

Figure 32: Experimental results at different locations and reduced frequency, at the height z = 0.5m.

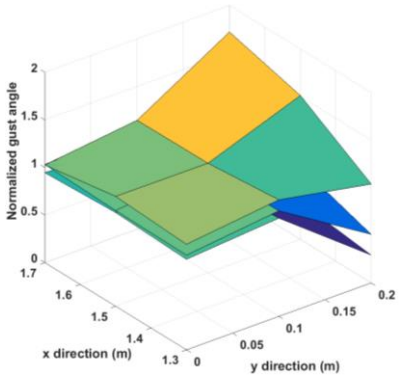

Figure 33: Experimental results at different locations and reduced frequency, at the height z = 1.5m.

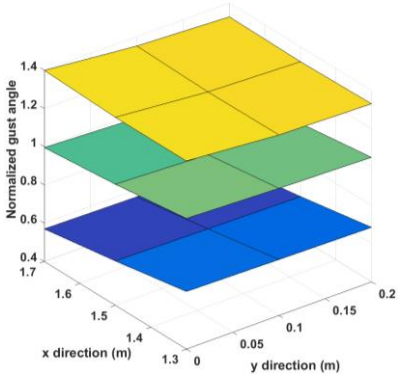

Figure 34: CFD results at different locations and reduced frequency.

While the CFD results are spatially uniform, the gust angle in the experimental results varies a lot when moving in transverse direction. This may be attributed to a shear region higher than predicted, created by the vanes turbulent boundary layer. This effect is higher at z = 0.5 m, which also support the evidence of the air falling when it flows out of the inlet.

3.4 Visual Observations

As stated at the beginning of section 3, a single hot-wire cannot provide sufficiently accurate measurements of the gust angle and, therefore, another technique to measure the gust angle has been used. By attaching a small string of wool flying freely in the flow, the flow direction can be evaluated, and thus the gust angle.

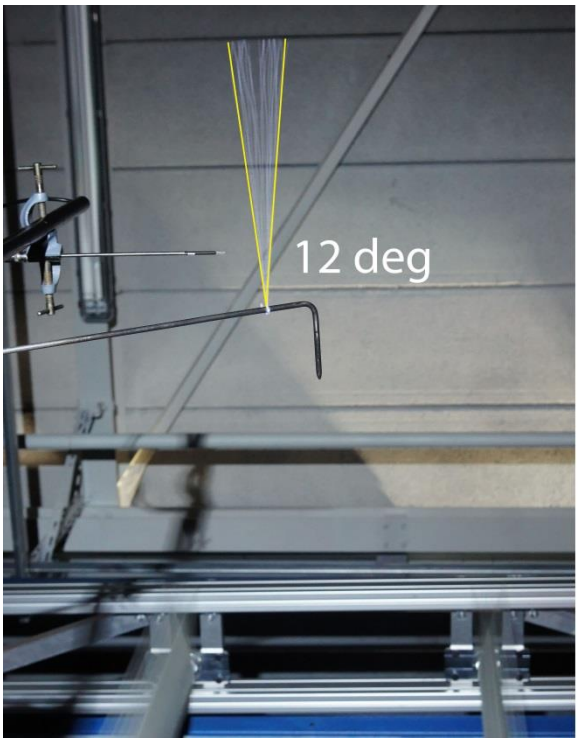

Figure 35: k = 0.0377 and δ_{max} = ±10 degrees.

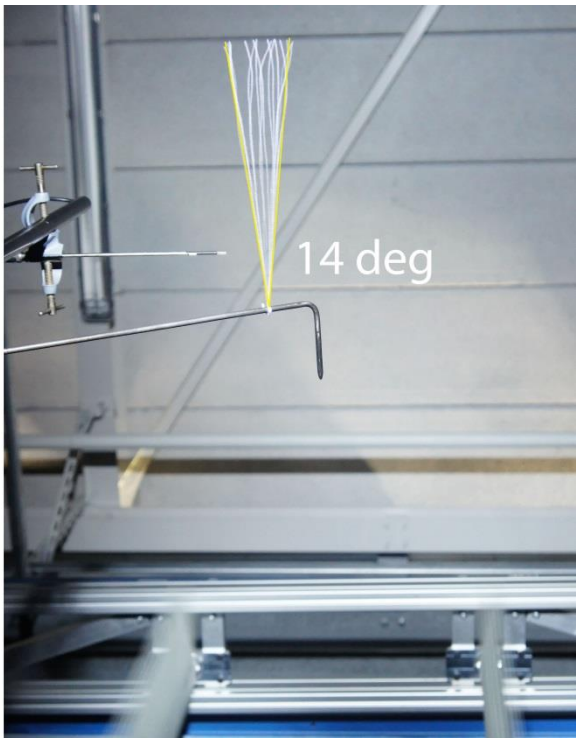

Figure 36: k = 0.1884 and δ_{max} = ±10 degrees.

Figure 35 and Figure 36 show a long exposure shot using stroboscopic light in the dark, to capture the variation of gust angle in time. The camera is located two meters below with an equivalent focal lens of 50 mm and an aperture of 6.51. The cone spanned by the string shows a time history of the flow direction and can be used as an estimate of the full amplitude of the gust (2 times the gust angle). The results are clearly higher than the CFD simulations and the measurements, with a gust angle evaluated at 6 degrees for k = 0.0377 and at 7 degrees for k = 0.1884 at z = 1.5m. The dependency relative to the reduced frequency can also be observed, but again, with a lower magnitude than predicted by the simulations.

Finally smoke visualization is done as shown in Figure 37 and Figure 38, in order to show the development of the gust in the wake. It is clear that the reduced frequency impacts the gust angle. Nonetheless, visual observations cannot be used for precise measurements, and an additional test campaign is required to fully evaluate the gust profile, by the means of particle image velocimetry and/or a cross wire anemometer.

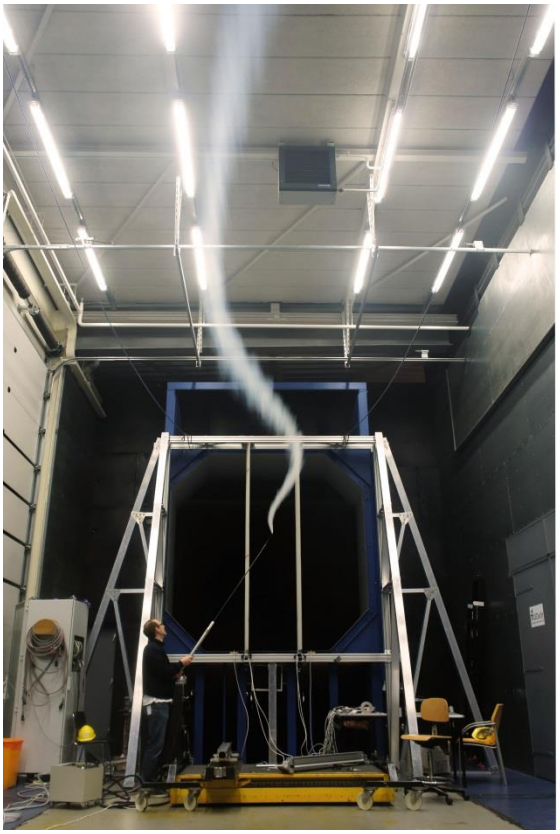

Figure 37: k = 0.1884 and δ_{max} = ±10 degrees.

Figure 38: k = 0.3768 and δ_{max} = ±10 degrees.

4 CONCLUSION

In this paper, the design of a gust generator developed at the Delft University of Technology and some preliminary results regarding its performance have been presented. The design phase consisted of high fidelity CFD simulations in order to identify the key design parameters acting on the gust flow. FSI simulations were performed to ensure that the actual structure meets the requirements. Results retrieved from the hot-wire anemometer are lower than the gust angle amplitude evaluated with CFD, but the visual observations revealed stronger gusts than both hot-wire measurements and numerical predictions. Such

discrepancies in the results can be associated with the inadequacy of the single hot wire probe for this type of flow measurement and with the fact that CFD simulations are done within a simplified fluid domain. Nonetheless, the relation between the gust angle and the vane deflection shows good agreement between experiment and numerical results, as well as a dependency of the gust on the reduced frequency. Measurements revealed also some important gust flow variation in height that will be corrected, by the adjunction of a "floor" at the same level of the flow inlet. The resonance issues with the frame will be solved by bolting it to the ground. Finally, this first trial assessed the proper operability of the overall system and highlighted required improvements for the next test sessions.

Once the gust profile will be fully evaluated in space, experiments will be realised on load alleviation and gust response. Besides of smart fixed wing, it is also believed that this gust generator could be helpful for wind turbine research and micro UAV development.

5 ACKNOWLEDGEMENT

The authors would like to thank Ron van Hoorn from Evonik for providing free foam samples, as well as to Ed Roessen, Roel Franken and Gertjan Mulder from the Delft University of Technology who provided help and invested some of their time in the construction of the gust generator. The help and support from Nico van Beek and Dr. Marios Kotsonis during the experiment at the OJF was deeply appreciated. Finally, the authors would like to thank Dr. Terence Macquart from the Delft University of Technology for his help on the control system and on the editing of this paper.

6 REFERENCES

[1] Tang D.M., Cizmas P.G.A., Dowell E.H., Experimental and analysis for a gust generator in a wind tunnel, *Journal of Aircraft*, 1996, 33, pp. 139–148

[2] Dequand S., Liauzun C., Girodroux-Lavigne P., Lepage A., Transonic response to a gust, *International Forum Of Aeroelasticity And Structural Dynamics*, Paris, Jun. 2011, Paper 374

[3] Neumann J., Mai H., Gust response: Simulation of an aeroelastic experiment by a fluid–structure interaction method, *Journal of Fluids and Structures*, 2013, 38, pp. 290–302

[4] Ricci S., Scotti A., Wind Tunnel Testing of an Active Controlled Wing under Gust Excitation, *49th AIAA/ASME/ASCE/AHS/ASC Structures, Structural Dynamics, and Materials Conference*, Schaumburg, IL, Apr. 2008, Paper 1727

[5] Dustin L. Grissom, William J. Devenport., Development and testing of a deterministic disturbance generator, *10th AIAA/CEAS Aeroacoustics Conference*, Manchester, May 2004, Paper 2956

[6] Wu Z.G., Chen L., Yang C., Study on gust alleviation control and wind tunnel test, *Sci China Tech Sci*, 2013, 56, pp. 762-771

[7] Saddington A.J., Finnis M.V., Knowles K., The characterisation of a gust generator for aerodynamic testing, *Proc IMechE Part G: J Aerospace Engineering*, 2014

[8] European Aviation Safety Agency: Certification Specifications for Normal, Utility, Aerobatic, and Commuter Category Aeroplanes CS23 Amendment 3, 2012, 1–C–2

7 COPYRIGHT STATEMENT